

Singlet O₂ Oxidation of a Deprotonated Guanine-Cytosine Base Pair and Its Entangling with Intra-Base-Pair Proton Transfer

Wenchao Lu,^[a, b] Yan Sun,^[a, b] Midas Tsai,^[c] Wenjing Zhou,^[a] and Jianbo Liu^{*[a, b]}

We report an experimental and computational study on the ¹O₂ oxidation of gas-phase deprotonated guanine-cytosine base pair [G·C–H][–] that is composed of 9HG·[C–H][–] and 7HG·[C–H][–] (pairing 9H- or 7H-guanine with N1-deprotonated cytosine), and 9HG·[C–H][–]_{PT} and 7HG·[C–H][–]_{PT} (formed by intra-base-pair proton transfer from the N1 of guanine to the N3 of [C–H][–]). The conformer-averaged reaction product ions and cross section were measured over a center-of-mass collision energy range from 0.1 to 0.5 eV using a guided-ion-beam tandem mass spectrometer. To explore conformation-specific reactivity, collision dynamics of ¹O₂ with each of the four [G·C–H][–] conformers was simulated at B3LYP/6-31G(d). Trajectories showed that the ¹O₂ oxidation of the base pair entangles with intra-base-pair

proton transfer, and prefers to occur in a collision when the base pair adopts a proton-transferred structure; trajectories also indicate that the 9HG-containing base pair favors stepwise formation of 4,8-endoperoxide of guanine, whereas the 7HG-containing base pair prefers concerted formation of guanine 5,8-endoperoxide. Using trajectory results as a guide, potential energy surfaces (PESs) along all possible reaction pathways were established using the approximately spin-projected ωB97XD/6-311++G(d,p)//B3LYP/6-311++G(d,p) method. PESs have not only rationalized trajectory findings but provided more accurate energetics and indicated that the proton-transferred base-pair conformers have lower activation barriers for oxidation than their non-proton-transferred counterparts.

1. Introduction

Singlet O₂[¹Δ_g]-generated oxidative damage to DNA initiates at guanine (G) nucleobases exclusively.^[1] The related guanine oxidation has been investigated in various structures (nucleobases, nucleosides, nucleotides, oligonucleotides, single-stranded and double-stranded DNA, and G-quadruplex DNA) and under different conditions, and reaction mechanism, kinetics and dynamics have been continuously revised with new findings.^[2] A commonly proposed mechanism is that deoxyguanosine (dGuo) is attacked by ¹O₂ on its imidazole ring, forming a transient endoperoxide that quickly converts to a hydroperoxide 8-OOHdGuo. 8-OOHdGuo within DNA is reduced to 8-oxo-7,8-dihydrodeoxyguanosine (OdGuo).^[2c,3] Free 8-OOHdGuo or that in short oligonucleotides, on the other hand, undergoes dehydration to oxidized 8-oxo-7,8-dihydro-deoxyguanosine (OdGuo^{ox}) and then rehydration to 5-hydroxy-8-oxo-7,8-dihydrodeoxyguanosine (5-OHdGuo). Under basic conditions, 5-OHdGuo goes through an acyl shift to produce spiroiminodihydantoin (dSp);^[4] while under acidic conditions,

the formation of *gem*-diol via a water addition to 5-OHdGuo becomes predominant.^[2f] Ring-opening of *gem*-diol at its N1–C6, accompanied with an intramolecular proton transfer, leads to a 4-carboxydGh. Decarboxylation of the latter yields 5-guanidinohydantoin (dGh).^[2f,i]

Despite that OdGuo was found as the major oxidation product for the guanine residues in double-stranded DNA, Burrows and co-workers have reported the non-reactivity of the guanine residues toward ¹O₂.^[5] They claimed that the π stacking around guanine sites sterically hinders the cycloaddition of ¹O₂, and the OdGuo detected in DNA may come from Type-I photooxidation.^[2r,5–6] On the other hand, Dumont *et al.* were able to observe the ¹O₂-oxidation of a 13 base-pair poly(dG-dC) in molecular dynamics simulations.^[2o,p]

We have recently reported the ¹O₂ oxidation dynamics and kinetics of guanine and 9-methylguanine (9MG, a guanosine prototype compound) in the gas phase^[7] and in aqueous solution.^[8] Transient endoperoxides and peroxides of guanine and 9MG were captured using guided-ion-beam scattering techniques, oxidation rate constants and product branching ratios were determined using online mass spectrometry and spectroscopy, and reaction mechanisms were delineated with the aid of dynamics simulations and reaction potential energy surfaces (PESs). In this work, we have extended our study to the deprotonated guanine-cytosine base pair ([G·C–H][–]) in the gas phase. Compared to isolated nucleobases, [G·C–H][–] serves as a more realistic model for probing the oxidatively generated damage to DNA residues. In view of the disputing results concerning the ¹O₂ oxidation of the guanine residues in DNA, this work was to clarify the intrinsic reactivity of base pair separated from surrounding structures.

[a] Dr. W. Lu, Y. Sun, W. Zhou, Prof. J. Liu
Department of Chemistry and Biochemistry, Queens College of the City University of New York, 65-30 Kissena Blvd., Queens, NY 11367, USA

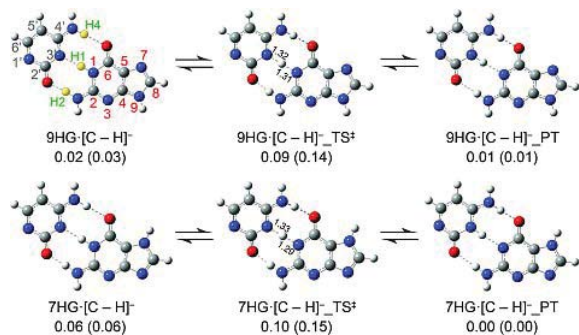
[b] Dr. W. Lu, Y. Sun, Prof. J. Liu
Ph.D. Program in Chemistry, the Graduate Center of the City University of New York,
365 5th Ave., New York, NY 10016, USA

[c] Prof. M. Tsai
Department of Natural Sciences, LaGuardia Community College, 31-10 Thomson Ave., Long Island City, NY 11101, USA

Supporting information for this article is available on the WWW under <https://doi.org/10.1002/cphc.201800643>

Another motivation for this work is that $[G\cdot C-H]^-$ suffices an ideal system to model the synergetic effects of ionization and oxidation. When ionizing radiation interacts with living organisms, the energy deposited in cells produces low-energy electrons. Accommodation of an extra electron into cytosine leads to dissociative electron attachment (DEA),^[9] i.e., the formation of a transient anion C^*- followed by ejecting a neutral H at the N1 position.^[10] When DEA and the ensuing dehydrogenation occur within G-C, deprotonated $[G\cdot C-H]^-$ is produced. The study of $[G\cdot C-H]^-$ oxidation is thus not only of significance to the fundamental understanding of DNA oxidative damage, but of practical interest in understanding the combined effects of radiotherapy and photodynamic therapy for cancer.^[11]

One structural complexity of gas-phase $[G\cdot C-H]^-$ arises from the mixing of 9H- and 7H-guanine tautomers, i.e., 9HG tautomer (population 24% at 298 K) with H atoms positioned at N1 and N9, and 7HG (69%) with the H atoms at N1 and N7.^[7a] Of the two tautomers, 9HG represents the correct guanine structure in nucleotide and DNA. Another complexity concerns with intra-base-pair proton transfer (PT) that is prompted by the deprotonation of C.^[12] PT relocates H and negative charge within $[G\cdot C-H]^-$; consequently, $[G\cdot C-H]^-$ is composed of four low-energy isomers (depicted in Scheme 1),



Scheme 1. Low-lying conformers of $[G\cdot C-H]^-$ and TSs for intra-base-pair PT, presented with numbering schemes and nomenclature. Reaction enthalpies (ΔH , eV) and free energy changes (ΔG , in parenthesis, eV) were calculated at ω B97XD/6-311++G(d,p)//B3LYP/6-311++G(d,p) with thermal corrections at 298 K. Hydrogen bonds are shown by dashed lines.

9HG \cdot [C-H]⁻ and 7HG \cdot [C-H]⁻ that are made by the Watson-Crick hydrogen bonding between neutral guanine and N1-deprotonated [C-H]⁻ and are henceforward referred to as conventional structures,^[13] and 9HG \cdot [C-H]⁻_PT and 7HG \cdot [C-H]⁻_PT that form by shuttling the H1 of guanine to the N3 site of [C-H]⁻,^[12] and thus are referred to as proton-transferred structures. The pair of conventional and proton-transferred conformers interconvert via an insignificant barrier (<0.1 eV).^[12a] The oxidation of $[G\cdot C-H]^-$ would thus entangle with guanine tautomerization and intra-base-pair PT. The consequences are that the actual ionization state of the guanine moiety hinges on intra-base-pair PT; and the change of the ionization state in turn alters the oxidation of guanine.^[7-8]

For a complex system like this, use of chemical intuition to predict reaction pathways may prove unreliable as there may exist multiple concurrent and competing processes.^[12b] A useful approach to identifying reaction pathways of $[G\cdot C-H]^-$ is quasi-classical, direct dynamics trajectory simulations.^[14] Direct dynamics trajectories explore multiple minima in the conformation landscape and the reaction PES. The motion of molecules is followed, allowing the molecules to show us what their preferred reaction pathways are. The direct dynamics method dispenses with PES; instead, it calculates energies, force constants and Hessians “on the fly” using quantum chemistry methods. This becomes computationally attractive for $[G\cdot C-H]^- + {}^1O_2$ that contains 30 atoms. Dynamics simulations partition the energy generated by oxidation to vibrational (E_{vib}), rotational (E_{rot}) and translational (E_{trans}) energy, increasing the chance of locating new reaction pathways.^[14g,ij] In addition, by following the variations of potential energy (PE) and bond lengths, we could identify better geometries for transition state (TS) searching.^[14g,h] As exemplified by our study on the dissociation of $[G\cdot C-H]^-$,^[12b] direct dynamics simulations act as a powerful guide to investigate base-pair chemistry and map out reaction coordinates and PESs.

The remainder of the paper is organized as follows: Section 2 describes the guided-ion-beam scattering experiment for measuring the reaction of $[G\cdot C-H]^-$ with 1O_2 , followed by the methodologies of direct dynamics simulations and PES calculations. Experimental reaction products, reaction cross section and their collision energy (E_{col}) dependence are reported in Section 3. Trajectory results of individual $[G\cdot C-H]^-$ conformers are presented in Section 4, from which possible reaction pathways were identified. Conformation-specific PESs along all possible reaction pathways were then constructed at higher levels of theory coupled with spin-contamination corrections, aimed at obtaining a more accurate description of reaction energetics. PES results are discussed in Section 5, along with their biological implications. Finally, conclusions are drawn in Section 6.

2. Experimental and Computational Details

2.1. Scattering of $[G\cdot C-H]^-$ by 1O_2 within a Guided-ion-beam Tandem Mass Spectrometer

Gas-phase reaction of $[G\cdot C-H]^-$ with 1O_2 was carried out on a home-made guided-ion-beam tandem mass spectrometer. The apparatus comprises an electrospray ionization (ESI) source, a radio frequency (rf) hexapole ion guide, a quadrupole mass filter, an rf octopole ion guide surrounded by a scattering cell, a second quadrupole mass filter, and a pulse-counting electron multiplier detector. Both quadrupole mass filters use Extrel 9.5 mm tri-filter rods and were operated at 2.1 MHz with a detectable m/z range of 1–500. Details of this apparatus were described elsewhere.^[15]

A sample solution of $[G\cdot C-H]^-$ was prepared in ethanol/water (v/v 3:1) containing 0.5 mM guanine (98%, Aldrich), 1.0 mM cytosine ($\geq 98\%$, Alfa Aesar) and 0.5 mM NaOH (reagent

grade, BDH). The solution was sprayed into ambient atmosphere through an electrospray needle at a flow rate of 0.06 mL/hr, and the ESI emitter was held at -2.3 kV. Charged droplets were introduced to the source chamber of the mass spectrometer through a capillary. The capillary was biased at -80 V and heated to 145 °C. Liquid droplets underwent desolvation as they passed through the heated capillary. Under mild heating conditions, both dry and hydrated $[G\cdot C-H]^-$ ions were produced in ion beam. A skimmer with an orifice of 1.0 mm is placed 3 mm from the capillary end, separating the source chamber and the hexapole ion guide. Ions were transported into the hexapole ion guide at a pressure of 24 mTorr, leading to collisional focusing and thermalization. Ions subsequently passed into a conventional quadrupole mass filter for selection of reactant ions. Mass-selected ions were collected and focused into the octopole ion guide that trapped ions in the radial direction and ran through a scattering cell containing 1O_2 . DC bias voltage was applied to the octopole, allowing control of the kinetic energy (E_{lab}) of reactant ions in the laboratory frame. E_{lab} can be converted into the center-of-mass E_{col} between collision partners using $E_{col} = E_{lab} \times m_{neutral} / (m_{ion} + m_{neutral})$, whereas $m_{neutral}$ and m_{ion} are the masses of neutral and ionic reactants, respectively.

To avoid the formation of radicals that accompany the photosensitized generation of 1O_2 ,^[16] 1O_2 was generated by $H_2O_2 + Cl_2 + 2KOH \rightarrow O_2$ ($\sim 85\%$ $X^3\Sigma_g^-$ and $\sim 15\%$ $a^1\Delta_g$) + $2KCl + 2H_2O$.^[17] Briefly, 10.5 mL of 8 M KOH (85%, Alfa Aesar) was slowly added to 20 mL of H_2O_2 (35 wt%, Alfa Aesar) in a sparger held at a temperature of -18 °C. 3.4 sccm of Cl_2 ($\geq 99.5\%$, Sigma-Aldrich) was mixed with 53.5 sccm of He and bubbled through the H_2O_2/KOH slush. Cl_2 completely reacted with H_2O_2 to produce 1O_2 , 3O_2 and water. The water vapor was removed after passing the gas products through a cold trap immersed in a methanol/water/dry ice slush of -70 °C. The mixture of 1O_2 , 3O_2 and He passed through an optical cell, where the 1O_2 emission of $a^1\Delta_g \rightarrow X^3\Sigma_g^-$ at 1270 nm^[18] and thus the 1O_2 concentration were measured using a calibrated InGaAs detector (Newport 71887, thermoelectrically cooled) coupled with a lock-in amplifier (SRS model SR830, paired with a SR540 chopper).^[17b] 1O_2 (mixed with 3O_2 and He) was then introduced into the scattering cell through a leak valve, and the cell pressure was measured by a capacitance manometer (MKS 690 head and 670 signal conditioner).

After ion-molecule scattering, remaining reactant ions and product ions drifted into the end of the octopole, mass analyzed by the second quadrupole and counted. Reaction cross section ($\sigma_{reaction}$) was calculated on the basis of the ratio of reactant and product ion intensities, the pressure of 1O_2 in the scattering cell (= cell pressure \times the concentration of 1O_2), and the effective cell length. The cell pressure was set to 0.25 mTorr, containing 6% of $^1O_2/^3O_2$ and 94% of He. Under these conditions, reactant ions had at most single collisions with O_2 . Ions also collided with He, but these collisions were insignificant due to the heavy-ion-light-neutral combination. To verify the non-reactivity of base-pair ions toward $^3O_2/He$, control experiment was performed under the same conditions except that Cl_2 was replaced by 3O_2 .

2.2. Direct Dynamics Simulations of Ion-Molecule Collisions

Trajectories were calculated for the collisions of 1O_2 with each of the four $[G\cdot C-H]^-$ conformers shown in Scheme 1. VENUS^[19] was used to set up initial conditions. A 300 K quasi-classical Boltzmann distribution^[20] was sampled for reactant E_{vib} (including zero-point energy ZPE) and E_{rot} . Trajectories were started with a center-of-mass separation of 8.0 Å between randomly-oriented base pair and 1O_2 . Relative velocities were added to reactants corresponding to the simulated E_{col} . The purpose of the simulations was to probe the gross features of base pair- 1O_2 collisions and identify reaction pathways, therefore all trajectories were calculated at zero impact parameter (i.e. head-on collisions).

Hessian-based predictor-corrector algorithm^[14f] implemented in Gaussian 09^[21] was used to integrate classical equations of motion, with Hessian recalculated every 5 steps. Trajectories were propagated with a step size of $0.25 \text{ amu}^{1/2} \text{ Bohr}$ (0.5–0.6 fs). A quadratically convergent SCF procedure^[22] was used in case the first-order SCF failed to converge. Because millions of gradients and Hessian evaluations were required, the theory used for the simulations had to be modest. B3LYP/6-31G(d) was chosen for the simulations as the PESs calculated using this theory were in reasonable agreement with those obtained from CASSCF(10,8).^[7b] The same theory was used successfully in the dynamics simulations of guanine,^[7a] 9MG,^[7b] and $[G\cdot C-H]^-$.^[12b] It was found that d polarization functions are necessary to correctly describe 1O_2 . A small batch of trajectories was repeated at B3LYP/6-31G(d,p) to test how a basis set with an explicit p polarization term for H atoms would affect intra-base-pair PT. The two sets of trajectories followed the same dynamics and produced the same product energy distributions, with the only difference being that the duration for intra-base-pair PT became shorter at B3LYP/6-31G(d,p).

Trajectories were terminated when product separation exceeded 9.0 Å or a maximum integration time (3.0 ps) was reached. A total of 800 trajectories were completed, each taking ~ 1500 CPU hrs. All calculations were completed on the computational clusters at Queens College and at CUNY High Performance Computing Center. gOpenMol^[23] was used for trajectory visualization. Analysis of trajectories was done with programs written for these purposes.

2.3. Electronic Structure Calculations of Reaction PESs and RRKM Analysis

Using trajectory results as a guide, structures for reactants, intermediates, TSs and products along all reaction pathways were optimized at B3LYP/6-311++G(d,p). All TSs were verified as first-order saddle points. Intrinsic reaction coordinate calculations were carried out to confirm that TSs are located between correct minima. As B3LYP/6-311++G(d,p) may underestimate the exoergicity of peroxides, single-point calculations were carried out at ω B97XD/6-311++G(d,p) using B3LYP optimized geometries. All reported energetics were based on the sum of ω B97XD/6-311++G(d,p) electronic energies and

B3LYP/6-311++G(d,p) thermal corrections at 298 K with ZPEs scaled by a factor of 0.988.^[24]

Note that due to the mixed open- and closed-shell characters of ${}^1\text{O}_2$,^[25] closed-shell calculations overestimate the ${}^1\text{O}_2$ excitation energy, whereas open-shell, broken-symmetry calculations bring about spin contamination from ${}^3\text{O}_2$. This problem exists for ${}^1\text{O}_2$ and its precursor complex and TS for the ${}^1\text{O}_2$ addition to guanine. To obtain accurate energetics in reaction PESs, we have adopted Yamaguchi's approximate spin projection^[26] to correct for spin contamination for early-stage structures in the PESs. Note that late-stage complexes and TSs (after ${}^1\text{O}_2$ addition) are dominated by single, closed-shell electronic states, thus spin contamination is no longer a serious issue. The spin-projected singlet-state electronic energy (E^{AP}) was calculated as

$$E^{\text{AP}} = \frac{E^{\text{BS}}\langle S^2 \rangle^{\text{HS}} - E^{\text{HS}}\langle S^2 \rangle^{\text{BS}}}{\langle S^2 \rangle^{\text{HS}} - \langle S^2 \rangle^{\text{BS}}} \quad (1)$$

where E refers to electronic energy, with the superscript AP representing the approximately spin-projected singlet state, BS the open-shell, broken-symmetry singlet state, and HS the triplet state; and $\langle S^2 \rangle$ indicates spin contamination. The so-calculated ${}^1\text{O}_2$ excitation energy is 1.02 eV, which agrees well with the experimental value of 0.98 eV.^[18] This spin-projection method has been used for the PESs of ${}^1\text{O}_2$ addition to guanine and 9MG,^[29,8] and calculated reaction barriers are consistent with experimental results.^[8]

Rice-Ramsperger-Kassel-Marcus (RRKM)^[27] density of states was calculated using the direct state count algorithm in the program of Zhu and Hase.^[28] The calculations used B3LYP/6-31G(d) frequencies and energies for the purpose of comparison with trajectory results calculated at the same level of theory.

3. Experimental Results of Ion-beam Scattering

We first measured the ${}^1\text{O}_2$ reaction with anhydrous $[\text{G}\cdot\text{C}-\text{H}]^-$ over an E_{col} range of 0.1–1.0 eV. However, no oxidation product was observed. Only collision-induced dissociation (CID) of $[\text{G}\cdot\text{C}-\text{H}]^-$ occurred at high E_{col} , leading to the detection of $[\text{G}-\text{H}]^-$ and $[\text{C}-\text{H}]^-$.^[12] The missing of oxidation products for bare $[\text{G}\cdot\text{C}-\text{H}]^-$ was not a real surprise since similar scenarios were observed in the ${}^1\text{O}_2$ reactions with bare protonated and deprotonated histidine,^[29] guanine,^[7a] 9MG^[7b] and 8-oxoguanine.^[30] All of these systems share a common feature in that reactions are mediated by the peroxides of an imidazole ring that were extremely unstable (with lifetime in the range of sub-ps to ps^[7,29–30]) and decayed back to starting reactants during the time-of-flight in the mass spectrometer.

To capture transient products for these oxidation reactions, we have devised a reaction routine by using hydrated reactant ions as the targets for collisions with ${}^1\text{O}_2$. The idea was to stabilize nascent peroxides on the basis of water evaporation cooling of peroxide products, as the elimination of water ligand would relax the exothermicity gained from peroxide formation. This strategy was proved to be successful in capturing the

oxidation products of histidine, guanine, 9MG and 8-oxoguanine. Following the same idea, we have measured the ${}^1\text{O}_2$ collisions with mono-hydrated $[\text{G}\cdot\text{C}-\text{H}]^-(\text{H}_2\text{O})$. Structures of the low-lying conformers of $[\text{G}\cdot\text{C}-\text{H}]^-(\text{H}_2\text{O})$ and their hydration energies ($E_{\text{hydration}}$) are provided in Figure S1 in the Supporting Information. Typical $E_{\text{hydration}}$ is 0.5–0.7 eV for reactants and ~ 0.5 eV for peroxides. The latter value is comparable to the reaction enthalpies for the oxidation of $[\text{G}\cdot\text{C}-\text{H}]^-$ (*vide infra*). The fact that the oxidation product for $[\text{G}\cdot\text{C}-\text{H}]^-(\text{H}_2\text{O}) + {}^1\text{O}_2$ was indeed detected in the experiment has supported our hypothesis.

Figure 1a shows a representative product ion mass spectrum measured as $E_{\text{col}}=0.1$ eV. Product ions at $m/z=293$ could

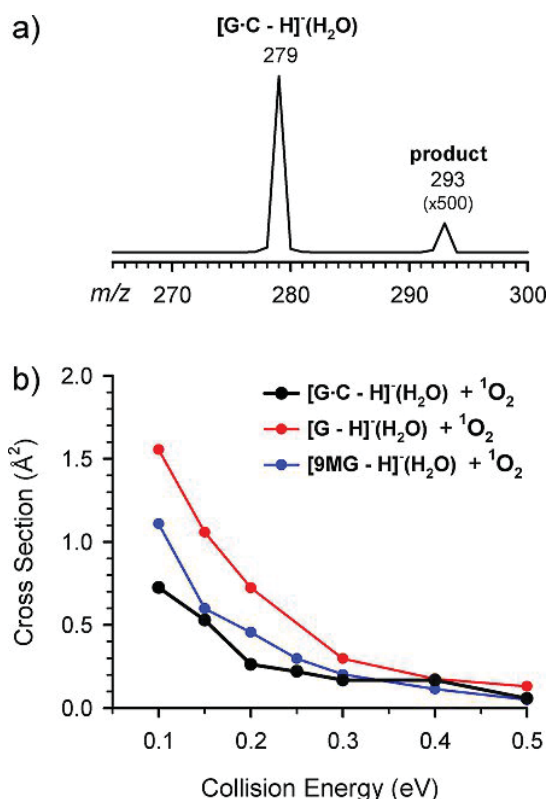


Figure 1. a) Product ion mass spectrum for the reaction of $[\text{G}\cdot\text{C}-\text{H}]^-(\text{H}_2\text{O}) + {}^1\text{O}_2$ measured at $E_{\text{col}}=0.1$ eV, and b) cross sections for the ${}^1\text{O}_2$ reactions with $[\text{G}\cdot\text{C}-\text{H}]^-(\text{H}_2\text{O})$, $[\text{G}-\text{H}]^-(\text{H}_2\text{O})$ and $[\text{9MG}-\text{H}]^-(\text{H}_2\text{O})$.

be attributed to the liberation of the water ligand from an O_2 adduct of $[\text{G}\cdot\text{C}-\text{H}]^-(\text{H}_2\text{O})$ ($m/z=279$). No peroxide was observed for intact $[\text{G}\cdot\text{C}-\text{H}]^-(\text{H}_2\text{O})$, neither for separated $[\text{G}-\text{H}]^-$ or $[\text{C}-\text{H}]^-$ — indicating that the ${}^1\text{O}_2$ oxidation of $[\text{G}\cdot\text{C}-\text{H}]^-$ did not lead to base-pair opening. Reaction cross section (σ_{reaction}) for $[\text{G}\cdot\text{C}-\text{H}]^-(\text{H}_2\text{O}) + {}^1\text{O}_2$ was plotted in Figure 1b, as a function of the center-of-mass E_{col} . For comparison, we have included in Figure 1b the reaction cross sections for ${}^1\text{O}_2$ with $[\text{G}-\text{H}]^-(\text{H}_2\text{O})$ and $[\text{9MG}-\text{H}]^-(\text{H}_2\text{O})$.^[7] Absolute uncertainty in reaction cross section measurement was estimated to be $\sim 20\%$, arising mostly from the measurement of ${}^1\text{O}_2$ concentration. But this

source of uncertainty did not affect relative cross sections, i.e. relative reactivities among different reactant ions and their E_{col} dependence. Relative uncertainty of cross sections was controlled to be less than 10% by averaging multiple sets of measurements.

Reaction cross sections for $[G\cdot C-H]^{-}(H_2O)$, $[G-H]^{-}(H_2O)$ and $[9MG-H]^{-}(H_2O)$ all increase with decreasing E_{col} , indicating that these reactions are exothermic with no barriers above the reactants. We have also measured the 1O_2 reaction with monohydrated $[9MG\cdot C-H]^{-}(H_2O)$ under the same conditions. However, the reaction cross section for $[9MG\cdot C-H]^{-}(H_2O) + ^1O_2$ was too small to allow for a meaningful measurement of E_{col} dependence. But the oxidation of $[9MG\cdot C-H]^{-}$ did appear to be exothermic, too.

The comparison between the oxidation of guanine nucleobases and base pair shows the order of reactivity as $[G-H]^{-} > [9MG-H]^{-} > [G\cdot C-H]^{-}$. Reaction efficiencies for these systems were estimated as the ratio of $\sigma_{reaction}/\sigma_{collision}$, where $\sigma_{collision}$ was taken as the greater of ion-induced dipole capture cross section^[31] and hard-sphere collision cross section. The results are 2.3% for $[G-H]^{-}(H_2O)$, 1.5% for $[9MG-H]^{-}(H_2O)$ and 0.6% for $[G\cdot C-H]^{-}(H_2O)$ at $E_{col}=0.1$ eV. The respective efficiencies drop to 1.5%, 0.6% and 0.2% at 0.2 eV. The fact that the reactivity of $[9MG-H]^{-}$ is much lower than that of $[G-H]^{-}$ has explained the extremely low efficiency we observed for $[9MG\cdot C-H]^{-}(H_2O)$ with 1O_2 .

To the best of our knowledge, there was no experimental assessment of the activation barrier for the 1O_2 oxidation of G-C base pair. The only relevant data was from Dumont *et al.*'s simulation, which predicted an activation barrier (ΔG^{\ddagger}) of 0.27 eV for the 1O_2 attack on the guanine residue within poly(dG-dC).^[2p] Our experiment has confirmed that the oxidation of $[G\cdot C-H]^{-}$ has no barriers above reactants, and the reaction is so exothermic that the reaction enthalpy is sufficient to remove a water ligand.

4. Trajectory Results

Among the Watson-Crick type conformers and tautomers of $[G\cdot C-H]^{-}$,^[12a] the four lowest-lying ones (see Scheme 1) are within the 0.1 eV energy and could all exist in the ion-beam experiment; therefore, trajectories for $[G\cdot C-H]^{-} + ^1O_2$ were initiated at each of the four conformers. A batch of 200 trajectories was collected for each starting base pair conforma-

tion. Trajectories were calculated at $E_{col}=0.1$ eV where the reaction probability was largest.

Figure S2 in the Supporting Information presents the 1O_2 collision positions for the trajectories of $9HG\cdot[C-H]^{-}_PT$, where the "instant of collision" was taken as the point for the first closest approach between O_2 and $9HG\cdot[C-H]^{-}_PT$. The probabilities for the 1O_2 collision with guanine, cytosine and intra-base-pair hydrogen bonds are 46%, 21% and 33%, respectively, in proportion to the target sizes. Similar distributions were produced in the trajectories of the other three conformers. This indicates that the trajectories did a reasonable job in randomly sampling collision orientations.

4.1. Intra-base-pair PT

One dynamics feature for $[G\cdot C-H]^{-}$ is intra-base-pair PT along $G(N1)-H1-C(N3)$ with equilibrium constant $K_{PT}(298\text{ K})=2.6$ for $9HG\cdot[C-H]^{-}\rightleftharpoons 9HG\cdot[C-H]^{-}_PT$ and 12.8 for $7HG\cdot[C-H]^{-}\rightleftharpoons 7HG\cdot[C-H]^{-}_PT$.^[12] Figure 2 has binned PT probability vs. trajectory time. Taking a snapshot at 200 fs, 20% of the $9HG\cdot[C-H]^{-}$ trajectories (Figure 2a) have transferred H1 once and 5% have transferred H1 twice. At the same trajectory time, 8% of $9HG\cdot[C-H]^{-}_PT$ (Figure 2b) have experienced single PT and 1% have double PT. The corresponding percentages are 23% and 3% for $7HG\cdot[C-H]^{-}$ (Figure 2c), and 14% and 4% for $7HG\cdot[C-H]^{-}_PT$ (Figure 2d). When approaching the collision instant, 45% of conventional conformers ($9HG\cdot[C-H]^{-}$ and $7HG\cdot[C-H]^{-}$) have PT; and the corresponding percentage is only 20–30% for proton-transferred conformers ($9HG\cdot[C-H]^{-}_PT$ and $7HG\cdot[C-H]^{-}_PT$). Apparently, the conventional structures present faster PT than the proton-transferred ones.

After collision, conformations have been scrambled, and PT thereafter happens randomly and independently of starting conformations. The PT probabilities counted at the end of trajectories are reported in Table 1. They are 54% for $9HG\cdot[C-H]^{-}$ and $9HG\cdot[C-H]^{-}_PT$, 77% for $7HG\cdot[C-H]^{-}$, and 50% for $7HG\cdot[C-H]^{-}_PT$. In a previous study, we have examined intra-base-pair PT in the collisions of $9HG\cdot[C-H]^{-}$ and $9HG\cdot[C-H]^{-}_PT$ with Ar at E_{col} of 3.0 and 5.0 eV.^[12b] The results are included in Table 1. Considering the similar sizes and masses of 1O_2 and Ar, the major difference in these collisions is the E_{col} used. It turns out that the PT probability for $9HG\cdot[C-H]^{-}$ decreases from 54% at 0.1 eV to 42% at 3.0 eV and 23% at 5.0 eV, and that for $9HG\cdot[C-H]^{-}_PT$ is 54% at 0.1 eV, 24% at 3.0 eV and 14% at 5.0 eV. Such E_{col} -dependence implies that PT

Table 1. Intra-base-pair PT probabilities in the collision trajectories of $[G\cdot C-H]^{-}$ with 1O_2 and Ar^a.

| Starting structure | 1O_2 collision at 0.1 eV | | Ar collision at 3.0 eV | | Ar collision at 5.0 eV | |
|------------------------|-----------------------------|-------------|------------------------|-------------|------------------------|-------------|
| | single PT | multiple PT | single PT | multiple PT | single PT | multiple PT |
| $9HG\cdot[C-H]^{-}$ | 21 ± 3% | 33 ± 4% | 31 ± 5% | 11 ± 4% | 18 ± 4% | 5 ± 2% |
| $9HG\cdot[C-H]^{-}_PT$ | 21 ± 3% | 33 ± 4% | 12 ± 4% | 12 ± 4% | 10 ± 3% | 4 ± 2% |
| $7HG\cdot[C-H]^{-}$ | 30 ± 4% | 44 ± 4% | – | – | – | – |
| $7HG\cdot[C-H]^{-}_PT$ | 14 ± 3% | 36 ± 4% | – | – | – | – |

^a Probabilities and uncertainties were calculated on the basis of 200 trajectories for each structure. Error limits are the statistical uncertainties calculated on the basis of the numbers of total trajectories and the number of PT trajectories.

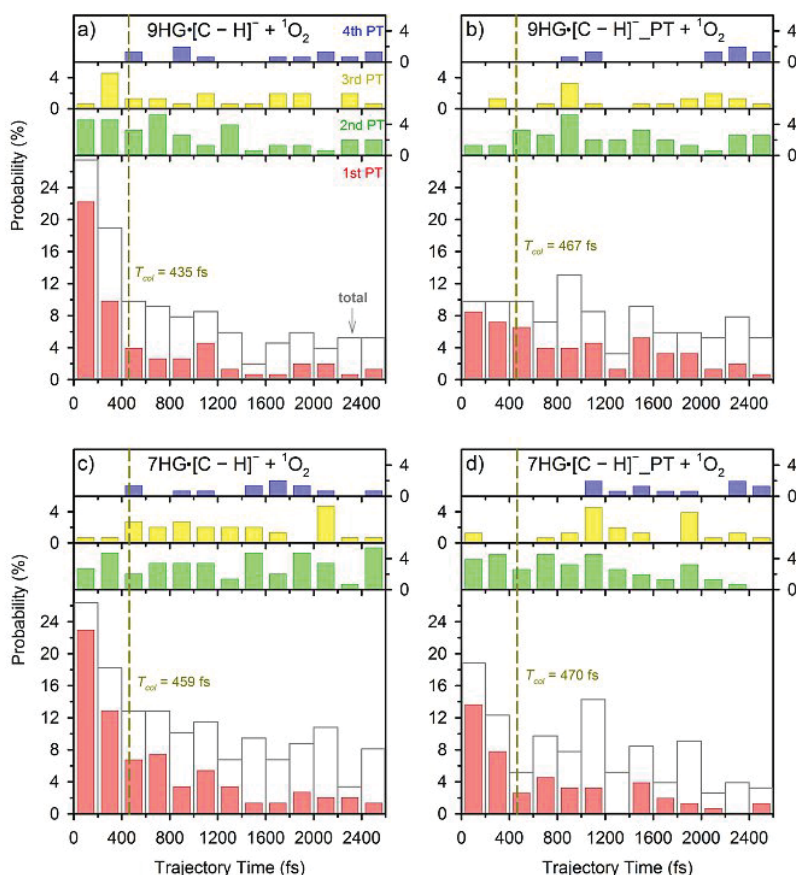


Figure 2. The probabilities of single, multiple and total intra-base-pair PT vs. trajectory time for a) $9\text{HG}\cdot[\text{C}-\text{H}]^-$, b) $9\text{HG}\cdot[\text{C}-\text{H}]^-_{\text{PT}}$, c) $7\text{HG}\cdot[\text{C}-\text{H}]^-$, and d) $7\text{HG}\cdot[\text{C}-\text{H}]^-_{\text{PT}}$. Bin size is 200 fs. Dark-yellow dashed lines indicate the instant of collision with $^1\text{O}_2$.

is nearly barrierless. The decreased PT at high E_{col} is due to the quick ending of trajectories at higher energies. A few trajectories have experienced PT along $\text{G}(\text{N}2)-\text{H}2-\text{C}(\text{O}2)$ and $\text{G}(\text{O}6)-\text{H}4-\text{C}(\text{N}4)$,^[12a] but the resulting structures are short-lived.

Finally, we calculated the ratio of different conformations at the end of trajectories. The results are $\frac{9\text{HG}\cdot[\text{C}-\text{H}]^-_{\text{PT}}}{9\text{HG}\cdot[\text{C}-\text{H}]^-} = 0.45$ for $9\text{HG}\cdot[\text{C}-\text{H}]^- + ^1\text{O}_2$ and 2.79 for $9\text{HG}\cdot[\text{C}-\text{H}]^-_{\text{PT}} + ^1\text{O}_2$; and $\frac{7\text{HG}\cdot[\text{C}-\text{H}]^-_{\text{PT}}}{7\text{HG}\cdot[\text{C}-\text{H}]^-} = 0.73$ for $7\text{HG}\cdot[\text{C}-\text{H}]^- + ^1\text{O}_2$ and 3.24 for $7\text{HG}\cdot[\text{C}-\text{H}]^-_{\text{PT}} + ^1\text{O}_2$. To figure out what conformation ratios would be expected from a statistical mechanism, we calculated the RRKM density of states at $E_{\text{col}} = 0.1$ eV. The density of states reflects the efficiency with which different conformers form and their populations if interconversion is facile. The density of states was calculated under the assumption that system energy has been randomized. The resulting RRKM conformation ratios are $\frac{9\text{HG}\cdot[\text{C}-\text{H}]^-_{\text{PT}}}{9\text{HG}\cdot[\text{C}-\text{H}]^-} = 5.5$ and $\frac{7\text{HG}\cdot[\text{C}-\text{H}]^-_{\text{PT}}}{7\text{HG}\cdot[\text{C}-\text{H}]^-} > 50$. The large deviation between trajectory and RRKM-predicted conformation ratios has thus implied the non-statistical nature of short-time collisions.

4.2. Dynamics for $^1\text{O}_2$ Attack

Consistent with the low reaction efficiency (0.6%) measured in the experiment, the probability for guanine oxidation is low even in head-on collision trajectories. Of the 800 trajectories we have calculated, $\sim 91\%$ belong to non-reactive, direct scattering with only one turning point in the relative motion of the reactant centers of mass. A typical direct-scattering trajectory for $9\text{HG}\cdot[\text{C}-\text{H}]^- + ^1\text{O}_2$ is illustrated in Figure 3. The top frame presents the changes in PE and the CM separation between collision partners throughout the trajectory. The middle frame shows the changes in product recoil energy (E_{recoil}) and E_{rot} . The bottom frame plots the changes in hydrogen bond lengths. The high-frequency oscillations in the PE and the hydrogen bond lengths reflect molecular vibrations. In this trajectory, the time during which $9\text{HG}\cdot[\text{C}-\text{H}]^-$ and $^1\text{O}_2$ are interacting strongly is 300 fs (highlighted by yellow-shaded area). At the collision instant, the repulsive potential converts E_{col} to a combination of PE, E_{vib} and E_{rot} . When the products are scattered, some of the PE is converted back to E_{recoil} , E_{rot} and E_{vib} . After the collision, the base pair undergoes PT along $\text{G}(\text{N}1)-\text{H}1-\text{C}(\text{N}3)$.

We have accumulated a total of 74 oxidation trajectories which could be grouped into two classes. The first class corresponds to the formation of a 4,8-endoperoxide of guanine

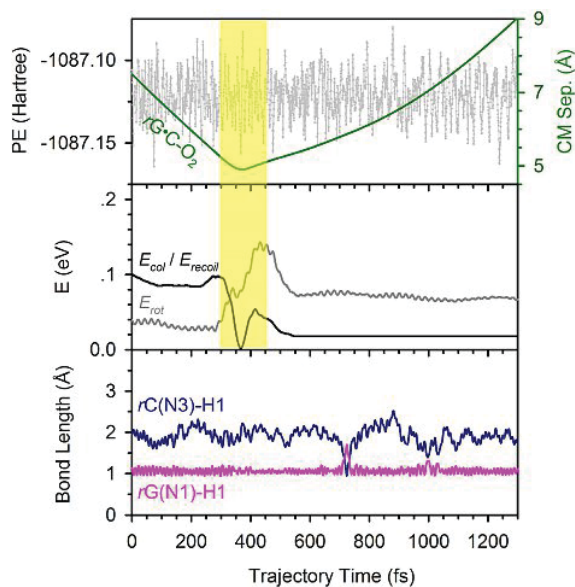


Figure 3. A representative non-reactive trajectory for $9\text{HG}\cdot[\text{C-H}]^- + {}^1\text{O}_2$ simulated at $E_{\text{col}} = 0.1$ eV. The top frame shows the changes of system PE and the CM separation between reactants; the middle frame shows the change of reactant E_{col} , product E_{recoil} and E_{rot} , and the bottom frame shows the variations of hydrogen bond lengths and accompanying PT. Yellow-shaded area indicates the moment when ${}^1\text{O}_2$ collides with $9\text{HG}\cdot[\text{C-H}]^-$. Video for the trajectory is available in the Supporting Information.

via stepwise ${}^1\text{O}_2$ addition, as demonstrated in Figure 4a and b. For the trajectory of $9\text{HG}\cdot[\text{C-H}]^- + {}^1\text{O}_2$ (Figure 4a), three instants are important: the onset of strong inter-reactant interaction at 700 fs (yellow-shaded area), the formation of an 8-peroxide at 900 fs, and the evolution to a 4,8-endoperoxide at 1350 fs (gray-shaded area). Formation of 4,8-endoperoxide also occurs to $9\text{HG}\cdot[\text{C-H}]^-_{\text{PT}} + {}^1\text{O}_2$ (Figure 4b). The nascent 4,8-endoperoxide is rather unstable, and the trajectories swing between 8-peroxide and 4,8-endoperoxide as indicated by the oscillations of $r\text{G}(\text{C}4)-\text{O}$ and $r\text{G}(\text{C}8)-\text{O}$. The same stepwise ${}^1\text{O}_2$ addition mechanism was observed in the dynamics simulation of $\text{B-DNA} + {}^1\text{O}_2$.^[2p]

The second class of oxidation trajectories can be characterized by concerted ${}^1\text{O}_2$ addition to guanine, which happens exclusively to the 7HG residue as demonstrated in Figure 4c and d. The trajectory of $7\text{HG}\cdot[\text{C-H}]^- + {}^1\text{O}_2$ (Figure 4c) shows sequential collision and oxidation. ${}^1\text{O}_2$ attacks $7\text{HG}\cdot[\text{C-H}]^-$ at

700 fs, followed by the formation of a 5,8-endoperoxide at 1400 fs. The oxidation is accompanied by the decrease of PE and the increase of E_{rot} (not shown). The trajectory of $7\text{HG}\cdot[\text{C-H}]^-_{\text{PT}} + {}^1\text{O}_2$ (Figure 4d) represents a similar concerted mechanism, except that ${}^1\text{O}_2$ addition is direct upon collision: ${}^1\text{O}_2$ impacts the base pair at 700 fs, and the two O synchronously anchor to the guanine C5 and C8 within 100 fs. It was found that 5,8-cycloaddition happens only at the times when the base pair adopts the $7\text{HG}\cdot[\text{C-H}]^-_{\text{PT}}$ conformation.

Table 2 summarizes the trajectory oxidation products and probabilities. The last two columns are the probabilities sorted on the basis of the base-pair conformations at the time when oxidation happened. Trajectories have revealed that the proton-transferred base-pair conformations are more prone to oxidation than their conventional structures, and the oxidation pathways of the base pair resemble those of isolated nucleobases (listed in the last two rows in the table).^[7b]

5. Reaction PESs and Biological Implications

Guided by the trajectory predicted reaction pathways, full reaction PESs for the four different conformers of $[\text{G}\cdot\text{C-H}]^-$ were constructed at the B3LYP level using a larger basis set $6-311 + \text{G}(\text{d},\text{p})$. To achieve more accurate reaction energetics, PESs were further refined by using single-point energy calculations at the $\omega\text{B97XD}/6-311 + \text{G}(\text{d},\text{p})$ level of theory, and the spin contaminations of ${}^1\text{O}_2$, precursor complexes and TS1s were corrected for by using the approximate spin projection method. Note that the TS1 for stepwise ${}^1\text{O}_2$ addition was calculated to be open-shell with $\langle S^2 \rangle = 0.959-0.965$, but that for concerted addition converged to closed-shell structures.

Figure 5 outlines the resulting reaction PESs, and each of Figure 5a and b plots two pathways that start from the conventional and the proton-transferred structures, respectively. For comparison, both reaction enthalpies (ΔH , eV) and free energy changes (ΔG , eV, in parentheses) at 298 K were presented in the PESs. The key points of the PESs are summarized as follows:

(1) The energetically most reactive conformer corresponds to $9\text{HG}\cdot[\text{C-H}]^-_{\text{PT}}$. Its oxidation follows a concerted addition mechanism as $9\text{HG}\cdot[\text{C-H}]^-_{\text{PT}} + {}^1\text{O}_2 \rightarrow \text{TS1} \rightarrow 8\text{-OOG}\cdot[\text{C-H}]^-_{\text{PT}} \rightarrow \text{TS2} \rightarrow 4,8\text{-OO-G}\cdot[\text{C-H}]^-_{\text{PT}}$. $8\text{-OOG}\cdot[\text{C-H}]^-_{\text{PT}}$ may also convert to $8\text{-OOHG}\cdot[\text{C-H}]^-_{\text{PT}}$ via TS3. We note that the hydration of $9\text{HG}\cdot[\text{C-H}]^-_{\text{PT}}$ lowers TS3 by 0.2 eV, as the water

Table 2. Trajectories results for the oxidation of $[\text{G}\cdot\text{C-H}]^-$ at $E_{\text{col}} = 0.1$ eV.

| Starting structure | Pathway and product | Probability ^a | | |
|---|---|--------------------------|--------------------|------------------------------|
| | | Total | at PT conformation | at conventional conformation |
| $9\text{HG}\cdot[\text{C-H}]^-$ | stepwise formation of 4,8-endoperoxide of guanine | $11 \pm 2\%$ | $7 \pm 2\%$ | $4 \pm 1\%$ |
| $9\text{HG}\cdot[\text{C-H}]^-_{\text{PT}}$ | | $8 \pm 2\%$ | $8 \pm 2\%$ | 0 |
| $7\text{HG}\cdot[\text{C-H}]^-$ | concerted formation of 5,8-endoperoxide of guanine | $10 \pm 2\%$ | $10 \pm 2\%$ | 0 |
| $7\text{HG}\cdot[\text{C-H}]^-_{\text{PT}}$ | | $8 \pm 2\%$ | $8 \pm 2\%$ | 0 |
| $[9\text{MG-H}]^-$ | same as $9\text{HG}\cdot[\text{C-H}]^- / 9\text{HG}\cdot[\text{C-H}]^-_{\text{PT}}$ | $15 \pm 3\%$ | – | – |
| $[7\text{HG-H}]^-$ | same as $7\text{HG}\cdot[\text{C-H}]^-_{\text{PT}}$ | $5 \pm 2\%$ | – | – |

^a Probabilities and uncertainties for base pairs were calculated on the basis of 200 trajectories for each structure.

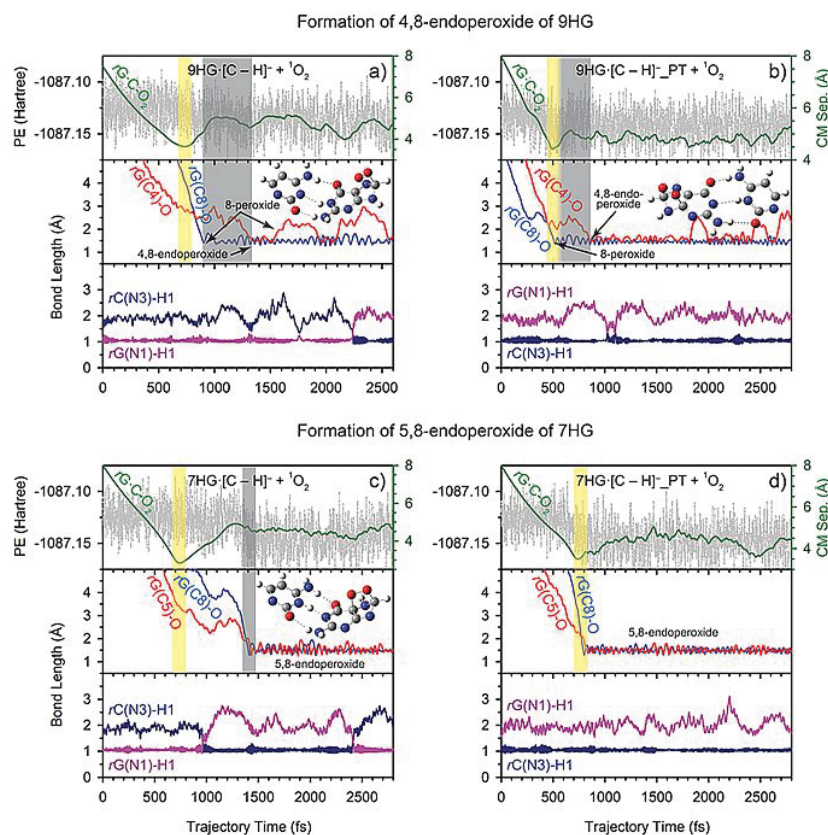


Figure 4. Representative trajectories for the $^1\text{O}_2$ oxidation of a) $9\text{HG}\cdot[\text{C}-\text{H}]^-$, b) $9\text{HG}\cdot[\text{C}-\text{H}]^-_{\text{PT}}$, c) $7\text{HG}\cdot[\text{C}-\text{H}]^-$, and d) $7\text{HG}\cdot[\text{C}-\text{H}]^-_{\text{PT}}$, simulated at $E_{\text{col}}=0.1$ eV. Each set, from the top frame, shows the changes of PE and the CM separation between reactants/products, the formation of peroxides (see inserted structures), the variations of hydrogen bond lengths, and intra-base-pair PT. Yellow-shaded areas indicate the collision moment, and gray-shaded areas show the moment when oxidation happens. Videos for the trajectories are available in the Supporting Information.

ligand would assist intramolecular PT.^[21] On the basis of reaction energetics, all of the $8\text{-OOG}\cdot[\text{C}-\text{H}]^-_{\text{PT}}$, $4,8\text{-OO-G}\cdot[\text{C}-\text{H}]^-_{\text{PT}}$ and $8\text{-OOHG}\cdot[\text{C}-\text{H}]^-_{\text{PT}}$ products may have contributed to the product ions we have detected in the ion-molecule experiment.

$9\text{HG}\cdot[\text{C}-\text{H}]^-$ follows the same stepwise pathway as its proton-transferred counterpart, but has higher barriers for the initial $^1\text{O}_2$ addition and for the subsequent evolution from 8-peroxide to 4,8-endoperoxide. The different PES energetics for $9\text{HG}\cdot[\text{C}-\text{H}]^-_{\text{PT}}$ vs. $9\text{HG}\cdot[\text{C}-\text{H}]^-$ are in good agreement with the different trajectory reaction probabilities reported for $9\text{HG}\cdot[\text{C}-\text{H}]^-_{\text{PT}}$ and $9\text{HG}\cdot[\text{C}-\text{H}]^-$ in Table 2.

(2) The concerted $^1\text{O}_2$ -cycloaddition mechanism dominates in the 7HG-containing base pairs. The cycloaddition reaction of $7\text{HG}\cdot[\text{C}-\text{H}]^-_{\text{PT}} + ^1\text{O}_2 \rightarrow 5,8\text{-OO-G}\cdot[\text{C}-\text{H}]^-_{\text{PT}}$ has an activation barrier $\Delta G(\text{TS}^\ddagger)$ of 0.61 eV. The barrier increases to 0.75 eV for $7\text{HG}\cdot[\text{C}-\text{H}]^- + ^1\text{O}_2$, which may be used to rationalize the fact that all 7HG-containing base pairs have the oxidation reaction occurring at their proton-transferred conformations.

(3) The NBO^[32] charges located on the guanine moieties of $7\text{HG}\cdot[\text{C}-\text{H}]^-_{\text{PT}}$ and $9\text{HG}\cdot[\text{C}-\text{H}]^-_{\text{PT}}$ were calculated to be -0.87 . These charges may facilitate the attack by electrophilic $^1\text{O}_2$ on the proton-transferred base-pair conformers.

(4) The ion beam scattering experiments have revealed a lower reactivity for $[\text{G}\cdot\text{C}-\text{H}]^-$ than free $[\text{G}-\text{H}]^-$. To reveal the origin of this reactivity difference, we have compared the rate-limiting activation barriers for the $^1\text{O}_2$ addition to different guanine structures. As shown in Table 3, the barriers for

Table 3. Activation barriers (eV) for the $^1\text{O}_2$ addition to different guanine structures^a.

| | $9\text{HG}\cdot[\text{C}-\text{H}]^-$ | $9\text{HG}\cdot[\text{C}-\text{H}]^-_{\text{PT}}$ | $7\text{HG}\cdot[\text{C}-\text{H}]^-$ | $7\text{HG}\cdot[\text{C}-\text{H}]^-_{\text{PT}}$ |
|--------------------------------|--|--|--|--|
| $\Delta H(\text{TS}^\ddagger)$ | 0.04 | -0.07 | 0.25 | 0.14 |
| $\Delta G(\text{TS}^\ddagger)$ | 0.49 | 0.34 | 0.75 | 0.61 |
| | 9HG | $[9\text{HG}-\text{H}]^-$ | 7HG | $[7\text{HG}-\text{H}]^-$ |
| $\Delta H(\text{TS}^\ddagger)$ | 0.40 | -0.22 | 0.68 | 0.00 |
| $\Delta G(\text{TS}^\ddagger)$ | 0.84 | 0.22 | 1.17 | 0.48 |

^a Calculated at $\omega\text{B97XD}/6\text{-311} + \text{G(d,p)}/\text{B3LYP}/6\text{-311} + \text{G(d,p)}$ with spin-projection corrections.

$\text{G}\cdot[\text{C}-\text{H}]^-_{\text{PT}}$ are higher than those for the corresponding isolated $[\text{G}-\text{H}]^-$ by ~ 0.15 eV. The increased barriers for $\text{G}\cdot[\text{C}-\text{H}]^-_{\text{PT}}$ implies that base pairing would to some extent shield nucleobases from $^1\text{O}_2$ damage. On the other hand, the conventional conformers $\text{G}\cdot[\text{C}-\text{H}]^-$ actually lower the activation

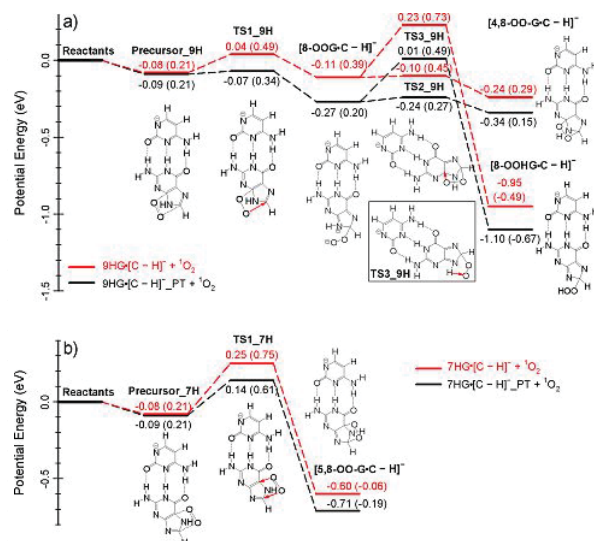


Figure 5. PESs for $^1\text{O}_2$ oxidation of a) $9\text{HG}\cdot[\text{C}-\text{H}]^-$ and $9\text{HG}\cdot[\text{C}-\text{H}]^-_{\text{PT}}$, and b) $7\text{HG}\cdot[\text{C}-\text{H}]^-$ and $7\text{HG}\cdot[\text{C}-\text{H}]^-_{\text{PT}}$. Reaction enthalpies (ΔH) and free energy changes (ΔG , in parenthesis) were calculated at $\omega\text{B97XD}/6-311++\text{G(d,p)}/\text{B3LYP}/6-311++\text{G(d,p)}$ with approximate spin-projection-based corrections for $^1\text{O}_2$, precursors and TS1 s, except that $[8-\text{OO-G-C-H}]^-$ was calculated at $\text{B3LYP}/6-311++\text{G(d,p)}$. Depicted structures refer to conventional conformers.

barriers compared to neutral G, but its biological implication is limited considering that the population of $\text{G}\cdot[\text{C}-\text{H}]^-$ is far less than $\text{G}\cdot[\text{C}-\text{H}]^-_{\text{PT}}$.

To examine the consequences of base pair oxidation, we have compared in Table 4 base-pair dissociation energy (ΔH_{diss}) and free energy changes (ΔG_{diss}). The oxidation of a conventional structure increases the dissociation energy, whereas the oxidation of a proton-transferred structure decreases it. Another consequence concerns the barrier for intra-base-pair PT (Table 4). While the barriers leading from the conventional structures have remained more or less the same, the barriers leading from the proton-transferred structures have increased upon oxidation. This finding has validated the trajectory results that in most oxidation trajectories the oxidized base pairs adopt proton-transferred structures at the end of trajectories.

6. Conclusions

A combined experimental and computational study was carried out for gas-phase deprotonated G·C base pair with $^1\text{O}_2$. O_2 adduct was captured as the only oxidation product of the base pair, and the reaction efficiency of the base pair is much less than that of free guanine. Trajectory simulations were initiated at each of the four base-pair conformers $9\text{HG}\cdot[\text{C}-\text{H}]^-$, $9\text{HG}\cdot[\text{C}-\text{H}]^-_{\text{PT}}$, $7\text{HG}\cdot[\text{C}-\text{H}]^-$ and $7\text{HG}\cdot[\text{C}-\text{H}]^-_{\text{PT}}$. Guided by the trajectories, conformation-specific reaction PESs were mapped out to address the biological consequences of different reactivities among various base pair structures and isolated nucleobases. It was found that the successive formation of 8-peroxide and 4,8-endoperoxide of the guanine moiety dominates in the oxidation of $9\text{HG}\cdot[\text{C}-\text{H}]^-$ and $9\text{HG}\cdot[\text{C}-\text{H}]^-_{\text{PT}}$, whereas the concerted formation of 5,8-endoperoxide of guanine is favored in the oxidation of $7\text{HG}\cdot[\text{C}-\text{H}]^-$ and $7\text{HG}\cdot[\text{C}-\text{H}]^-_{\text{PT}}$. The oxidation prefers to occur at the time when the base pair adopts a proton-transferred conformation.

Supporting Information

Structures of $[\text{G}\cdot\text{C}-\text{H}]^-(\text{H}_2\text{O})$; collision sites in the trajectories of $9\text{HG}\cdot[\text{C}-\text{H}]^-_{\text{PT}} + ^1\text{O}_2$; oxidation PES of the cytosine moiety in $[\text{G}\cdot\text{C}-\text{H}]^-$; Cartesian coordinates of the structures in Scheme 1 and in Figures 5, S1 and S3; videos for the trajectories in Figures 3 and 4.

Acknowledgements

This work was supported by the National Science Foundation Award (Grant No. CHE-1464171) and Queens College Research Enhancement Award. The authors thank William Hase (Texas Tech University) for assistance with Venus. WL acknowledges the CUNY Mina Rees Dissertation Fellowship. WZ acknowledges the Queens College Trudy Rothman Chemistry Award.

Conflict of Interest

The authors declare no conflict of interest.

| Table 4. Base-pair dissociation energies (ΔH_{diss} and ΔG_{diss} , eV) and barriers (TS [‡] , eV) for intra-base-pair PT ^a . | | | | | | | | | |
|--|--------------------------|--------------------------|--------------------------------|--------------------------------|--|--------------------------|--------------------------|--------------------------------|--------------------------------|
| Structure | ΔH_{diss} | ΔG_{diss} | $\Delta H(\text{TS}^\ddagger)$ | $\Delta G(\text{TS}^\ddagger)$ | Structure | ΔH_{diss} | ΔG_{diss} | $\Delta H(\text{TS}^\ddagger)$ | $\Delta G(\text{TS}^\ddagger)$ |
| $9\text{HG}\cdot[\text{C}-\text{H}]^-$ | 1.69 | 1.16 | 0.04 | 0.26 | $7\text{HG}\cdot[\text{C}-\text{H}]^-$ | 1.64 | 1.12 | 0.07 | 0.21 |
| $9\text{HG}\cdot[\text{C}-\text{H}]^-_{\text{PT}}$ | 1.72 | 1.18 | 0.10 | 0.21 | $7\text{HG}\cdot[\text{C}-\text{H}]^-_{\text{PT}}$ | 1.61 | 1.09 | 0.09 | 0.21 |
| $8-\text{OO}-9\text{HG}\cdot[\text{C}-\text{H}]^-$ | 1.97 ^b | 1.43 ^b | 0.03 | 0.06 | $5,8-\text{OO}-7\text{HG}\cdot[\text{C}-\text{H}]^-$ | 2.11 | 1.57 | 0.00 | 0.04 |
| $8-\text{OO}-9\text{HG}\cdot[\text{C}-\text{H}]^-_{\text{PT}}$ | 1.50 | 0.98 | 0.18 | 0.24 | $5,8-\text{OO}-7\text{HG}\cdot[\text{C}-\text{H}]^-_{\text{PT}}$ | 1.46 | 0.94 | 0.17 | 0.23 |
| $4,8-\text{OO}-9\text{HG}\cdot[\text{C}-\text{H}]^-$ | 1.97 | 1.43 | 0.02 | 0.06 | | | | | |
| $4,8-\text{OO}-9\text{HG}\cdot[\text{C}-\text{H}]^-_{\text{PT}}$ | 1.52 | 1.02 | 0.14 | 0.22 | | | | | |
| $8-\text{OOH}-9\text{HG}\cdot[\text{C}-\text{H}]^-$ | 2.17 | 1.62 | 0.01 | 0.05 | | | | | |
| $8-\text{OOH}-9\text{HG}\cdot[\text{C}-\text{H}]^-_{\text{PT}}$ | 1.49 | 0.98 | 0.17 | 0.24 | | | | | |

^a Calculated at $\text{B3LYP}/6-311++\text{G(d,p)}$. ^b $8-\text{OO}-9\text{HG}$ converged to $4,8-\text{OO}-9\text{HG}$ upon base-pair separation.

Keywords: singlet oxygen · guanine-cytosine base pair · guided-ion-beam tandem mass spectrometry · direct dynamics trajectory simulation · potential energy surface

- [1] F. Prat, C.-C. Hou, C. S. Foote, *J. Am. Chem. Soc.* **1997**, *119*, 5051-5052.
- [2] a) C. Sheu, C. S. Foote, *J. Am. Chem. Soc.* **1993**, *115*, 10446-10447; b) C. J. Burrows, J. G. Muller, *Chem. Rev.* **1998**, *98*, 1109-1151; c) J.-L. Ravanat, P. Di Mascio, G. R. Martinez, M. H. G. Medeiros, J. Cadet, *J. Biol. Chem.* **2000**, *275*, 40601-40604; d) J. C. Niles, J. S. Wishnok, S. R. Tannenbaum, *Org. Lett.* **2001**, *3*, 963-966; e) P. Kang, C. S. Foote, *J. Am. Chem. Soc.* **2002**, *124*, 4865-4873; f) Y. Ye, J. G. Muller, W. Luo, C. L. Mayne, A. J. Shallop, R. A. Jones, C. J. Burrows, *J. Am. Chem. Soc.* **2003**, *125*, 13926-13927; g) J. E. B. McCallum, C. Y. Kuniyoshi, C. S. Foote, *J. Am. Chem. Soc.* **2004**, *126*, 16777-16782; h) M. R. Ilesca, F. Cermola, F. Temussi, *Curr. Org. Chem.* **2005**, *9*, 109-139; i) W. L. Neeley, J. M. Essigmann, *Chem. Res. Toxicol.* **2006**, *19*, 491-505; j) J. Cadet, J.-L. Ravanat, G. R. Martinez, M. H. G. Medeiros, P. Di Mascio, *Photochem. Photobiol.* **2006**, *82*, 1219-1225; k) J.-L. Ravanat, G. R. Martinez, M. H. G. Medeiros, P. Di Mascio, J. Cadet, *Tetrahedron* **2006**, *62*, 10709-10715; l) B. H. Munk, C. J. Burrows, H. B. Schlegel, *J. Am. Chem. Soc.* **2008**, *130*, 5245-5256; m) J. Cadet, T. Douki, J.-L. Ravanat, *Acc. Chem. Res.* **2008**, *41*, 1075-1083; n) J. Cadet, T. Douki, J.-L. Ravanat, *Free Radical Biol. Med.* **2010**, *49*, 9-21; o) E. Dumont, R. Grüber, E. Bignon, C. Morell, Y. Moreau, A. Monari, J.-L. Ravanat, *Nucleic Acids Res.* **2016**, *44*, 56-62; p) E. Dumont, R. Grüber, E. Bignon, C. Morell, J. Aranda, J.-L. Ravanat, I. Tuñón, *Chem. Eur. J.* **2016**, *22*, 12358-12362; q) B. Thapa, B. H. Munk, C. J. Burrows, H. B. Schlegel, *Chem. Eur. J.* **2017**, *23*, 5804-5813; r) A. M. Fleming, C. J. Burrows, *Free Radical Biol. Med.* **2017**, *107*, 35-52.
- [3] S. Frelon, T. Douki, J.-L. Ravanat, J.-P. Pouget, C. Tornabene, J. Cadet, *Chem. Res. Toxicol.* **2000**, *13*, 1002-1010.
- [4] J.-L. Ravanat, G. R. Martinez, M. H. G. Medeiros, P. Di Mascio, J. Cadet, *Arch. Biochem. Biophys.* **2004**, *423*, 23-30.
- [5] A. M. Fleming, C. J. Burrows, *Chem. Res. Toxicol.* **2013**, *26*, 593-607.
- [6] R. P. Hickerson, F. Prat, J. G. Muller, C. S. Foote, C. J. Burrows, *J. Am. Chem. Soc.* **1999**, *121*, 9423-9428.
- [7] a) W. Lu, J. Liu, *Chem. Eur. J.* **2016**, *22*, 3127-3138; b) W. Lu, H. Teng, J. Liu, *Phys. Chem. Chem. Phys.* **2016**, *18*, 15223-15234.
- [8] W. Lu, Y. Sun, W. Zhou, J. Liu, *J. Phys. Chem. B* **2018**, *122*, 40-53.
- [9] B. Boudaiffa, P. Cloutier, D. Hunting, M. A. Huels, L. Sanche, *Science* **2000**, *287*, 1658-1660.
- [10] a) H. Abdoul-Carime, S. Gohlke, E. Illenberger, *Phys. Rev. Lett.* **2004**, *92*, 168103/1-168103/4; b) S. Denifl, S. Ptasińska, M. Probst, J. Hrušák, P. Scheier, T. D. Märk, *J. Phys. Chem. A* **2004**, *108*, 6562-6569.
- [11] A. Colasanti, A. Kisslinger, M. Quarto, P. Riccio, *Acta Biochim. Pol.* **2004**, *51*, 1039-1046.
- [12] a) W. Lu, J. Liu, *Phys. Chem. Chem. Phys.* **2016**, *18*, 32222-32237; b) J. Liu, *Phys. Chem. Chem. Phys.* **2017**, *19*, 30616-30626.
- [13] M. C. Lind, P. P. Bera, N. A. Richardson, S. E. Wheeler, H. F. Schaefer, III, *Proc. Natl. Acad. Sci.* **2006**, *103*, 7554-7559.
- [14] a) R. Car, M. Parrinello, *Phys. Rev. Lett.* **1985**, *55*, 2471-2474; b) K. K. Baldrige, M. S. Gordon, R. Steckler, D. G. Truhlar, *J. Phys. Chem.* **1989**, *93*, 5107-5119; c) T. Helgaker, E. Uggerud, H. J. A. Jensen, *Chem. Phys. Lett.* **1990**, *173*, 145-150; d) K. Bolton, W. L. Hase, *Modern Methods for Multidimensional Dynamics Computations in Chemistry* **1998**, 143-189; e) W. L. Hase, JAI, Greenwich, **1998**; f) V. Bakken, J. M. Millam, H. B. Schlegel, *J. Chem. Phys.* **1999**, *111*, 8773-8777; g) M. Döntgen, M.-D. Przybylski-Freund, L. C. Kröger, W. A. Kopp, A. E. Ismail, K. Leonhard, *J. Chem. Theory Comput.* **2015**, *11*, 2517-2524; h) E. Martínez-Núñez, *Phys. Chem. Chem. Phys.* **2015**, *17*, 14912-14921; i) S. Pratihari, X. Ma, Z. Homayoon, G. L. Barnes, W. L. Hase, *J. Am. Chem. Soc.* **2017**, *139*, 3570-3590; j) X. Ma, W. L. Hase, *Philos. Trans. R. Soc., A* **2017**, *375*, 20160204/1-20160204/20.
- [15] Y. Fang, J. Liu, *J. Phys. Chem. A* **2009**, *113*, 11250-11261.
- [16] C. Schweitzer, R. Schmidt, *Chem. Rev.* **2003**, *103*, 1685-1757.
- [17] a) A. Midey, I. Dotan, A. A. Viggiano, *J. Phys. Chem. A* **2008**, *112*, 3040-3045; b) Y. Fang, F. Liu, A. Bennett, S. Ara, J. Liu, *J. Phys. Chem. B* **2011**, *115*, 2671-2682.
- [18] W. J. Lafferty, A. M. Solodov, C. L. Lugez, G. T. Fraser, *Appl. Opt.* **1998**, *37*, 2264-2270.
- [19] a) W. L. Hase, K. Bolton, P. de Sainte Claire, R. J. Duchovic, X. Hu, A. Komornicki, G. Li, K. Lim, D. Lu, G. H. Peslherbe, K. Song, K. N. Swamy, S. R. Vande Linde, A. Varandas, H. Wang, R. J. Wolf, Texas Tech University Lubbock, TX, **1999**; b) X. Hu, W. L. Hase, T. Pirraglia, *J. Comput. Chem.* **1991**, *12*, 1014-1024.
- [20] G. H. Peslherbe, H. Wang, W. L. Hase, *Adv. Chem. Phys.* **1999**, *105*, 171-201.
- [21] M. J. Frisch, G. W. Trucks, H. B. Schlegel, G. E. Scuseria, M. A. Robb, J. R. Cheeseman, G. Scalmani, V. Barone, B. Mennucci, G. A. Petersson, H. Nakatsuji, M. Caricato, X. Li, H. P. Hratchian, A. F. Izmaylov, J. Bloino, G. Zheng, J. L. Sonnenberg, M. Hada, M. Ehara, K. Toyota, R. Fukuda, J. Hasegawa, M. Ishida, T. Nakajima, Y. Honda, O. Kitao, H. Nakai, T. Vreven, J. J. A. Montgomer, J. E. Peralta, F. Ogliaro, M. Bearpark, J. J. Heyd, E. Brothers, K. N. Kudin, V. N. Staroverov, T. Keith, R. Kobayashi, J. Normand, K. Raghavachari, A. Rendell, J. C. Burant, S. S. Iyengar, J. Tomasi, M. Cossi, N. Rega, J. M. Millam, M. Klene, J. E. Knox, J. B. Cross, V. Bakken, C. Adamo, J. Jaramillo, R. Gomperts, R. E. Stratmann, O. Yazyev, A. J. Austin, R. Cammi, C. Pomelli, J. W. Ochterski, R. L. Martin, K. Morokuma, V. G. Zakrzewski, G. A. Voth, P. Salvador, J. J. Dannenberg, S. Dapprich, A. D. Daniels, O. Farkas, J. B. Foresman, J. V. Ortiz, J. Cioslowski, D. J. Fox, Gaussian, Inc, Wallingford, CT, **2013**.
- [22] G. B. Bacskay, *Chem. Phys.* **1981**, *61*, 385-404.
- [23] L. Laaksonen, 3.0 ed., Center for Scientific Computing, Espoo, Finland, **2005**, p. available at www.csc.fi/gopenmol/.
- [24] M. P. Andersson, P. Uvdal, *J. Phys. Chem. A* **2005**, *109*, 2937-2941.
- [25] A. Maranzana, G. Ghigo, G. Tonachini, *J. Am. Chem. Soc.* **2000**, *122*, 1414-1423.
- [26] a) T. Saito, S. Nishihara, Y. Kataoka, Y. Nakanishi, T. Matsui, Y. Kitagawa, T. Kawakami, M. Okumura, K. Yamaguchi, *Chem. Phys. Lett.* **2009**, *483*, 168-171; b) T. Saito, S. Nishihara, Y. Kataoka, Y. Nakanishi, Y. Kitagawa, T. Kawakami, S. Yamanaka, M. Okumura, K. Yamaguchi, *J. Phys. Chem. A* **2010**, *114*, 7967-7974.
- [27] R. A. Marcus, *J. Chem. Phys.* **1952**, *20*, 359-364.
- [28] L. Zhu, W. L. Hase, Chemistry Department, University of Indiana, Bloomington, **1993**.
- [29] F. Liu, W. Lu, Y. Fang, J. Liu, *Phys. Chem. Chem. Phys.* **2014**, *16*, 22179-22191.
- [30] Y. Sun, W. Lu, J. Liu, *J. Phys. Chem. B* **2017**, *121*, 956-966.
- [31] J. Troe, *Chem. Phys. Lett.* **1985**, *122*, 425-430.
- [32] E. D. Glendening, J. K. Badenhop, A. E. Reed, J. E. Carpenter, J. A. Bohmann, C. M. Morales, C. R. Landis, F. Weinhold, Theoretical Chemistry Institute, University of Wisconsin, Madison, WI, **2013**.

Manuscript received: July 5, 2018
Accepted Article published: July 26, 2018
Version of record online: August 9, 2018